First results on a search for light pseudoscalar sgoldstino in K^- decays

I.V. Ajinenko, S.A. Akimenko, I.G. Britvich, G.I. Britvich, K.V. Datsko, A.P. Filin, A.V. Inyakin, A.S. Konstantinov, V.F. Konstantinov, I.Y. Korolkov, V.M. Leontiev, V.P. Novikov, V.F. Obraztsov, V.A. Polyakov, V.I. Romanovsky, V.I. Shelikhov, N.E. Smirnov, O.G. Tchikilev, E.V. Vlasov, O.P. Yushchenko.

Institute for High Energy Physics, Protvino, Russia

V.N. Bolotov, S.V. Laptev, V.A. Lebedev, A.R. Pastsjak, A.Yu. Polyarush, R.Kh. Sirodeev.

Institute for Nuclear Research Moscow, Russia

arXiv:hep-ex/0212060 v1   25 Dec 2002

Abstract

A search for the light pseudoscalar sgoldstino production in three-body K^- decay $K^- \to \pi^- \pi^0 \, P$ has been performed with the "ISTRA+" detector exposed to the 25 GeV negative secondary beam of the U-70 proton synchrotron. No signal is seen. Upper limits for the branching ratio $Br(K^- \to \pi^- \pi^0 P)$ at 90% confidence level vary between $2.0 \cdot 10^{-5}$ and $0.5 \cdot 10^{-5}$ in the effective mass m_P range from 0 up to 190 MeV. Our results improve the limits published by the E787 Collaboration in the mass interval between 0 and 120 MeV and are the first ones at higher masses.

1 Introduction

In supersymmetric models with spontaneous supersymmetry breaking superpartners of a Goldstone fermion — goldstino, pseudoscalar P and scalar S, should exist. In various versions of gravity mediated and gauge mediated theories one or both of these weakly interacting bosons — sgoldstinos — are light and therefore can be observed in kaon decays. Moreover, if sgoldstino interactions with quarks conserve parity,(as in left-right extensions of MSSM), and P is lighter than S, so that $m_S > (m_K - m_\pi)$ and $m_P < (m_K - 2m_\pi)$, sgoldstinos show up in the decay $K \to \pi\pi P$, rather than in much better constrained $K \to \pi S$. The phenomenology of light sgoldstinos in this scenario is considered in details in [1]. Under assumption that sgoldstino interactions with quarks and gluons violate quark flavor and conserve parity, low energy interactions of pseudoscalar sgoldstino P with quarks are described by the Lagrangian:

$$L = -P \cdot (h_{ij}^D \cdot \overline{d}_i i\gamma^5 d_j + h_{ij}^U \cdot \overline{u}_i i\gamma^5 u_j) \tag{1}$$

with

$$d_i = (d, s, b) \,, \qquad u_i = (u, c, t) \,, \tag{2}$$

with coupling constants h_{ij} proportional to the left-right soft terms in the matrix of squared masses of squarks:

$$h_{ij}^D = \frac{\tilde{\mathrm{m}}_{D,ij}^{(LR)2}}{\sqrt{2}F} \,, \qquad h_{ij}^U = \frac{\tilde{\mathrm{m}}_{U,ij}^{(LR)2}}{\sqrt{2}F} \,, \tag{3}$$

Here the scale of supersymmetry breaking is denoted as $\sqrt{F}$. The constraints on the flavor-violating coupling of sgoldstino to quarks is evaluated using the $K_L^\circ - K_S^\circ$ mass difference and CP violating parameter ϵ in the neutral kaon system: $|h_{12}^D| \leq 7 \cdot 10^{-8}; |Reh_{12}^D \cdot Imh_{12}^D| < 1.5 \cdot 10^{-17}$. It has been shown in [1] that, depending on the phase of sgoldstino-quark coupling, these constraints result in the following limits on the branching ratio: $Br(K^- \to \pi^- \pi^0 P) \leq 1.5 \times 10^{-6} \div 4 \times 10^{-4}$ (see Fig. 1 for the diagram of the K^- decay). A search for P in charged kaon decays is of particular interest for the case $Reh_{12}^D \sim 0$, when the corresponding branching ratio of K_L is small.

Light sgoldstino decays into two photons or into a pair of charged leptons, two photon decay dominating almost everywhere in the parameter space. Depending on the parameter $g_\gamma = \frac{1}{2\sqrt{2}}\frac{M_{\gamma\gamma}}{F}$, where $M_{\gamma\gamma}$ is the photino mass, sgoldstino decays either inside or outside the detector. In the present search we assume that sgoldstino decays outside the detector, i.e is invisible. The existing limits on the branching $Br(K^- \to \pi^- \pi^0 P)$ are at the level of $4 \cdot 10^{-5}$ [2], whereas the limits for the scalar sgoldstino S can be estimated from the studies of the $K^+ \to \pi^+ \nu\overline{\nu}$ at the level of $4.7 \cdot 10^{-9}$, see [3] for recent review.

The aim of our present study is to search for invisible pseudoscalar sgoldstino in the decay of K^-. Experimental setup and event selection are described in Section 2, the results of the analysis are presented in Section 3 and the conclusions are given in the last Section.

2 Experimental setup and event selection

2.1 Experimental setup

The experiment is performed at the IHEP 70 GeV proton synchrotron U-70. The spectrometer ISTRA+ has been described in some details in our recent papers on K_{e3} [4], $K_{\mu3}$ [5] and $\pi^- \pi^\circ \pi^\circ$ decays [6], here we briefly

recall characteristics relevant to our analysis. The 40 m spectrometer ISTRA+ is located in the negative unseparated secondary beam line 4A of U-70. The beam momentum is ~ 25 GeV with $\Delta p/p \sim 2\%$. The admixture of K^- in the beam is $\sim 3\%$, the beam intensity is $\sim 3 \cdot 10^6$ per 1.9 sec U-70 spill. A schematic view of the ISTRA+ setup is shown in Fig. 2. The momentum of a beam particle deflected by the magnet M_1 is measured by four proportional chambers BPC_1—BPC_4 with 1 mm wire step, the kaon identification is done by three threshold Cerenkov counters $\check{C}_1$—$\check{C}_3$. The 9 meter long vacuumated decay volume is surrounded by eight lead glass rings used to veto low energy photons. The same role is played by 72-cell lead glass calorimeter SP_2. The decay products deflected in the magnet M_2 with 1 Tm field integral are measured with 2 mm step proportional chambers PC_1—PC_3, with 1 cm cell drift chambers DC_1—DC_3 and finally with 2 cm diameter drift tubes DT_1—DT_4. A wide aperture threshold Cerenkov counter $\check{C}_4$ is filled with He and used to trigger electrons. SP_1 is a 576-cell lead glass calorimeter, followed by HC — a scintillator-iron sampling hadron calorimeter. MH is a 11x11 cell scintillating hodoscope, used to solve ambiguity for multitrack events and improve the time resolution of the tracking system, MuH is a 7x7 cell muon hodoscope.

The trigger is provided by scintillation counters S_1—S_5, beam Cerenkov counters and by the analog sum of amplitudes from last dinodes of the SP_1 : $T=S_1 \cdot S_2 \cdot S_3 \cdot \overline{S}_4 \cdot \check{C}_1 \cdot \overline{\check{C}}_2 \cdot \overline{\check{C}}_3 \cdot \overline{S}_5 \cdot \Sigma(SP_1)$, here S_4 is a scintillation counter with a hole to suppress beam halo, S_5 is a counter downstream of the setup at the beam focus, $\Sigma(SP_1)$ - a requirement for the analog sum to be larger than a MIP signal. ,

During first run in March-April 2001, 363 million of trigger events were logged on DLT's. During second physics run in November-December 2001 350 million trigger events were collected with higher beam intensity and somewhat stronger trigger requirements. This information is supported by about 100 million MC events generated using Geant3 [7] for dominant K^- decay modes. Signal efficiency for possible sgoldstino production has been estimated using one million generated events for the first run configuration and 0.5 million events for the second run configuration, for each effective mass m_P point in the mass interval from 0 to 200 MeV with a step of 10 MeV. These signal events were weighted using the matrix element given in [1].

2.2 Event selection

Data collected in two runs, Spring 2001, first run, and Winter 2001, second run, are used. Some information on the data processing and reconstruction procedures is given in [4, 5, 6], here we briefly mention the details, relevant for $\pi^-\pi^\circ$ + missing energy event selection.

The muon identification (see [5]) is based on the information from the SP_1 — a 576-cell lead glass calorimeter and the HC — a scintillation-iron sampling calorimeter. The electron identification (see [4]) is done using E/p ratio — of the energy of the shower associated with charged track and charged track momentum.

A set of cuts is designed in order to suppress various backgrounds to possible sgoldstino production:

0) Events with one reconstructed charged track and with two electromagnetic showers in the electromagnetic calorimeter SP_1 are selected. We require the effective mass $m(\gamma\gamma)$ to be within ± 40 MeV from m_{π°. The effective two-photon mass distributions for two runs are shown in Fig. 3. Events with vertex inside interval $400 < z < 1650$ cm are selected.

1) Next cut is a "soft" charged pion identification, tracks having electron or muon flag (as described in [4, 5]) are rejected.

2) Events with missing energy $E_{beam} - E_{\pi^-} - E_{\pi^\circ}$ below 3 GeV are rejected. The cut on the missing energy serves to reduce $K_{\pi 2}$ contribution. In Fig. 4 missing energy spectra for the second run data, MC background and MC signal with m_P of 90 MeV are compared.

3) Events with $m(\gamma\gamma)$ within ± 36 MeV from $m_{\pi^\circ} 135$ MeV a selected (Tough π° cut).

4) Fourth cut suppresses events with extra photons irradiated by charged particles in a detector material upstream M2-magnet. Such photons have nearly the same x coordinate on the SP_1 face as the charged track, i.e event is rejected if at least one photon has $|x_{ch} - x_\gamma| < 10$ cm.

5) Fifth cut removes events having good K_{e3} 2C-fit.

6) The following cut is a restriction on the charged pion momentum p^* in the kaon rest frame: $p^*(\pi^-) <$ 180 MeV. It is designed to suppress the tails of the $K_{\pi 2}$ decay.

7) Seventh cut is against remaining muon contamination.It is required that the energy in SP_1, associated with charged track, should exceed 0.7 GeV. This cut requires "early" hadron shower in SP_1 and has , unfortunately,

low signal efficiency. We plan to get rid of it in our final analysis.

8) The following cut is designed to suppress $\pi^-\pi^\circ\gamma$ contribution: only the events with missing momentum crossing SP_1 transverse plane within SP_1 working aperture are selected.

9) The "Veto" cut uses information from the Guard System GS and the guard electromagnetic calorimeter SP_2: absence of signals above noise threshold is required. The influence of the "Veto" cut on the two-photon effective mass spectrum is illustrated in Fig. 5. No π° signal is seen after the "Veto" cut.

10) As a result of the previous cuts, π°-signal practically disappears from the $\gamma\gamma$ mass spectrum. This allows to perform effective linear background subtraction procedure. The interval $\pm$ 18 MeV around m(π°) mass value is used as the signal region, remaining events are used for the background estimate.

The data reduction information is given in Table 1 for two runs and is compared in Tables 2,3 with MC-background statistics and with MC-signal statistics for the sgoldstino mass of $m = 90$ MeV.

The influence of the last eight cuts on the missing mass squared spectrum $(P_K - P_{\pi^-} - P_{\pi^\circ})^2$, which is used as the signal "estimator" is is shown in Fig. 6 for the second run data. The left wide bump in Fig. 6 is due to $K_{\mu 3}$ decays, the shift to negative missing mass squared is caused by the use of the pion mass in its calculations. Second peak is caused by $\pi^-\pi^\circ(\pi^\circ)$ decay with gammas from second π° escaping detection.

Fig. 7 illustrates the background subtraction procedure: in the first(third) figure the missing mass squared spectrum after cut 10 is shown for the first(second) run (solid curve) together with the normalized background(dashed curve) estimated from the $m(\gamma\gamma)$ spectrum side bands (99–117 MeV and 153–171 MeV). The second(forth) figure show signal-background difference for two runs. No sgoldstino signal is observed, the peak around 0.02 GeV^2 is due to remaining $\pi^-\pi^\circ(\pi^\circ)$ background.

Table 1: Event reduction statistics for two runs.

Cut	Events run 1	N_i/N_{i+1}	Events run 2	N_i/N_{i+1}
(0) 1 π^- and m($\gamma\gamma$) near m(π°)	4398982		11339975	
(1) no (e, μ)	978752	1.48	8762220	1.29
(2) $E_{mis} > 3.0$ GeV	716830	4.16	1430781	6.12
(3) narrow m($\gamma\gamma$) band	581653	1.23	1297087	1.10
(4) conv. gammas	322073	1.81	723248	1.79
(5) no K_{e3} fit	230424	1.40	487246	1.48
(6) $p^*(\pi^-) < 180$ MeV	150926	1.53	322298	1.51
(7) $E_{SP_1} > 700$ MeV	17101	8.83	51624	6.24
(8) 10 < rr < 60 cm	12922	1.32	40356	1.28
(9) Veto	5255	2.46	11183	3.61
(10) $\pm$18 meV	2691	1.95	6125	1.94

3   Analysis and results

In order to calculate the upper limits we have fitted the residual missing mass distribution by the sum of the background and the signal Gaussian with fixed width of $\sigma = 0.003$ GeV^2, as determined from the signal MC.

The signal MC is also used to determine the efficiency of our cuts. The background has been described by two components: the Gaussian for $\pi^-\pi^\circ(\pi^\circ)$ peak and a linear background. For the second run an additional wide Gaussian centered at -0.015 has been used. Fit results are illustrated in Fig. 7 for the first and second run, respectively.

The upper limits at the 90% confidence level are calculated from the value

$$N_{UL} = N_{obs} + 1.64 \cdot \sigma \quad , \tag{4}$$

3

Table 2: Event reduction statistics for MC data, first run.

Cut	Events mix MC	N_i/N_{i+1}	MC signal with m=90 MeV	N_i/N_{i+1}
(0) 1 π^- and m($\gamma\gamma$) near m(π°)	1278382		207315	
(1) no (e, μ)	1156685	1.11	203841	1.02
(2) E$_{mis}$ > 3.0 GeV	158181	7.31	168179	1.21
(3) narrow m($\gamma\gamma$) band	149679	1.06	165105	1.02
(4) conv. gammas	91251	1.64	94503	1.75
(5) no K_{e3} fit	48067	1.90	68325	1.38
(6) $p^*(\pi^-)$ < 180 MeV	32151	1.50	67528	1.01
(7) E_{SP_1} > 700 MeV	6880	4.67	22346	3.02
(8) 10 < rr < 60 cm	5283	1.30	17883	1.25
(9) Veto	2257	2.34	17770	1.01
(10) $\pm$18 MeV	1521	1.48	15737	1.13

where N_{obs} is the number of events in the signal Gaussian. During the fit we impose the constraint that N_{obs} is nonnegative. Sigma is a non-Gaussian error in N_{obs}. The upper limit UL is calculated as

$$UL = \frac{N_{UL} \cdot 0.2116 \cdot 0.98798 \cdot \varepsilon(K_{\pi 2})}{N(K_{\pi 2}) \cdot \varepsilon} \qquad (5)$$

with 0.2116 equal to $Br(K_{\pi 2})$; with 0.98798 equal to $Br(\pi^\circ \to \gamma\gamma)$ and $N(K_{\pi 2})$ equal to the number of reconstructed $\pi^-\pi^\circ$ decays found to be 1500000 events for the first run and 4500000 events for the second run.

The values ε and $\varepsilon(K_{\pi 2})$ are respective acceptances for $K^- \to \pi^-\pi^\circ P$ and $K_{\pi 2}$ decays. The acceptance $\varepsilon(K_{\pi 2})$ is equal to 17.49 % for the first run and 24.92 % for the second run. This acceptance includes both the reconstruction efficiency and geometrical acceptance. The results of the fits are given in Table 4. As the background conditions for the two runs are different, the first run provides better upper limits for some m_P regions regardless of the lower luminosity. The estimated systematic errors for the upper limits are at the level of 20 %.

The final result obtained using combined statistics of two runs is given in Table 5. The weighted ratio $\varepsilon(K_{\pi 2})/\varepsilon$ with the weights proportional to the runs statistics has been used for the combined data sample. Fig. 9 shows a comparison of our result with that published by the E787 collaboration [2].

Special attention should be paid to the region near m_{π° mass. If we assume that the sgoldstino mass is exactly equal to that of π° and that the remaining π° peak is due to sgoldstino signal, then the upper limit for this point is $2.8 \cdot 10^{-4}$.

4 Summary and conclusions

A search for a possible pseudoscalar sgoldstino production in the decay $K^- \to \pi^-\pi^\circ P$ has been performed. It was assumed that sgoldstino decays outside the setup, i.e is invisible. No signal is seen in the m_P mass interval between 0 and 200 MeV. The 90% confidence upper limits obtained vary between $2.0 \cdot 10^{-5}$ and $0.5 \cdot 10^{-5}$ for the sgoldstino mass range of $0 \div 190$ MeV. These results improve the confidence limits published by the E787 Collaboration.

In future, we plan to extend our search for a sgoldstino signal in the scenario when the decay $P \to \gamma\gamma$ happens inside the setup.

The authors would like to thank D.S. Gorbunov, V.A. Matveev, V.A. Rubakov, for numerous discussions.

The INR part of the collaboration is supported by the RFFI fund contract N00-02-16074.

Table 3: Event reduction statistics for MC data, second run.

Cut	Events mix MC	N_i/N_{i+1}	MC signal with m=90 MeV	N_i/N_{i+1}
(0) 1 π^- and m($\gamma\gamma$) near m(π°)	5117109		120594	
(1) no (e, μ)	4627156	1.11	119292	1.01
(2) E$_{mis}$ > 3.0 GeV	618446	7.48	98098	1.22
(3) narrow m($\gamma\gamma$) band	565772	1.09	96504	1.02
(4) conv. gammas	346226	1.63	54206	1.78
(5) no K_{e3} fit	118536	2.92	37124	1.46
(6) $p^*(\pi^-)$ < 180 MeV	114160	1.04	36835	1.01
(7)E_{SP_1} > 700 MeV	21824	5.23	11800	3.12
(8) 10 < rr < 60 cm	16597	1.28	9462	1.25
(9) Veto	7229	2.30	9407	1.01
(10) ±18 MeV	5114	1.41	8541	1.10

Table 4: Mass dependence of upper limits UL calculated using two runs separately, left part — first run, right part second run.

M, MeV	Eff. ε, %	$N_{obs} \pm \sigma$	UL	Eff. ε, %	$N_{obs} \pm \sigma$	UL
0	0.64	0±4.80	$1.84 \cdot 10^{-5}$	0.85	0±17.51	$2.39 \cdot 10^{-5}$
10	0.66	0±4.76	$1.76 \cdot 10^{-5}$	0.86	0±17.90	$2.40 \cdot 10^{-5}$
20	0.67	0±4.65	$1.69 \cdot 10^{-5}$	0.92	0±16.81	$2.10 \cdot 10^{-5}$
30	0.74	0±4.49	$1.48 \cdot 10^{-5}$	0.99	0±14.88	$1.73 \cdot 10^{-5}$
40	0.81	0±4.32	$1.30 \cdot 10^{-5}$	1.05	0±12.32	$1.65 \cdot 10^{-5}$
50	0.88	0±4.19	$1.16 \cdot 10^{-5}$	1.18	0±9.73	$1.56 \cdot 10^{-5}$
60	1.05	0±4.19	$0.98 \cdot 10^{-5}$	1.32	0±7.67	$1.10 \cdot 10^{-5}$
70	1.09	0±4.51	$1.01 \cdot 10^{-5}$	1.73	0±6.35	$0.70 \cdot 10^{-5}$
80	1.21	0±5.71	$1.15 \cdot 10^{-5}$	1.62	0±5.62	$0.66 \cdot 10^{-5}$
90	1.33	0±10.97	$2.02 \cdot 10^{-5}$	1.76	0±5.26	$0.57 \cdot 10^{-5}$
100	1.41	0±24.59	$4.24 \cdot 10^{-5}$	1.90	0±5.40	$0.54 \cdot 10^{-5}$
110	1.53	10.96±18.16	$3.96 \cdot 10^{-5}$	2.09	0±6.86	$0.62 \cdot 10^{-5}$
120	1.60	17.22±15.99	$2.24 \cdot 10^{-5}$	2.27	0±12.44	$1.04 \cdot 10^{-5}$
130	1.63	0±25.86	$3.86 \cdot 10^{-5}$	2.36	0±28.13	$2.26 \cdot 10^{-5}$
140	1.66	0±25.72	$3.79 \cdot 10^{-5}$	2.46	0±27.42	$2.12 \cdot 10^{-5}$
150	1.61	8.27±22.97	$4.25 \cdot 10^{-5}$	2.49	0 ±24.85	$1.89 \cdot 10^{-5}$
160	1.74	0±14.91	$2.33 \cdot 10^{-5}$	2.41	0±20.96	$1.65 \cdot 10^{-5}$
170	1.48	0±20.95	$3.46 \cdot 10^{-5}$	2.35	0±19.98	$1.61 \cdot 10^{-5}$
180	1.42	0±21.00	$3.60 \cdot 10^{-5}$	2.18	15.0±13.35	$1.61 \cdot 10^{-5}$
190	1.27	0±16.19	$3.11 \cdot 10^{-5}$	2.01	0±29.29	$2.77 \cdot 10^{-5}$
200	0.85	0±15.89	$4.54 \cdot 10^{-5}$	1.26	6.49±15.96	$3.00 \cdot 10^{-5}$

Table 5: Mass dependence of upper limits UL calculated using two runs together.

M, MeV	$N_{obs} \pm \sigma$	UL
0	0±11.21	$1.85 \cdot 10^{-5}$
10	0±11.05	$1.78 \cdot 10^{-5}$
20	0±10.56	$1.61 \cdot 10^{-5}$
30	0±9.72	$1.37 \cdot 10^{-5}$
40	0±8.62	$1.14 \cdot 10^{-5}$
50	0±7.42	$0.88 \cdot 10^{-5}$
60	0±6.39	$0.68 \cdot 10^{-5}$
70	0±5.78	$0.58 \cdot 10^{-5}$
80	0±5.69	$0.49 \cdot 10^{-5}$
90	0±6.27	$0.50 \cdot 10^{-5}$
100	0±7.88	$0.58 \cdot 10^{-5}$
110	0±12.59	$0.85 \cdot 10^{-5}$
120	0±25.67	$1.61 \cdot 10^{-5}$
130	0±19.91	$1.20 \cdot 10^{-5}$
140	0±15.51	$0.91 \cdot 10^{-5}$
150	0±14.94	$0.87 \cdot 10^{-5}$
160	0±16.79	$0.99 \cdot 10^{-5}$
170	0±17.07	$1.03 \cdot 10^{-5}$
180	0±20.09	$1.31 \cdot 10^{-5}$
190	0±22.12	$1.57 \cdot 10^{-5}$
200	13.66±19.06	$3.08 \cdot 10^{-5}$

References

[1] D.S. Gorbunov and V.A. Rubakov, Phys. Rev. **D64** (2001) 054008.

[2] S. Adler et al., E787 Collaboration, Phys. Rev. **D63** (2001) 032004.

[3] L. Littenberg, Rare kaon and pion decays, Lectures given at the PSI Summer School on Particle Physics, Zuoz, 2002, preprint hep-ex/0212005.

[4] I.V. Ajinenko et al., Study of the $K^- \to \pi^\circ e^- \nu$ decay, IHEP preprint 2001-051(2001); hep-ex/0112023,2001.

[5] I.V. Ajinenko et al., Study of the $K^- \to \mu^- \nu \pi^\circ$ decay, IHEP preprint 2002-6(2002).

[6] I.V. Ajinenko et al., Measurement of the Dalitz plot slope parameters for $K^- \to \pi^\circ \pi^\circ \pi^-$ decay using ISTRA+ detector, IHEP preprint 2002-16, Protvino, 2002.

[7] R. Brun et al, CERN-DD/EE/84-1, CERN, Geneva, 1984.
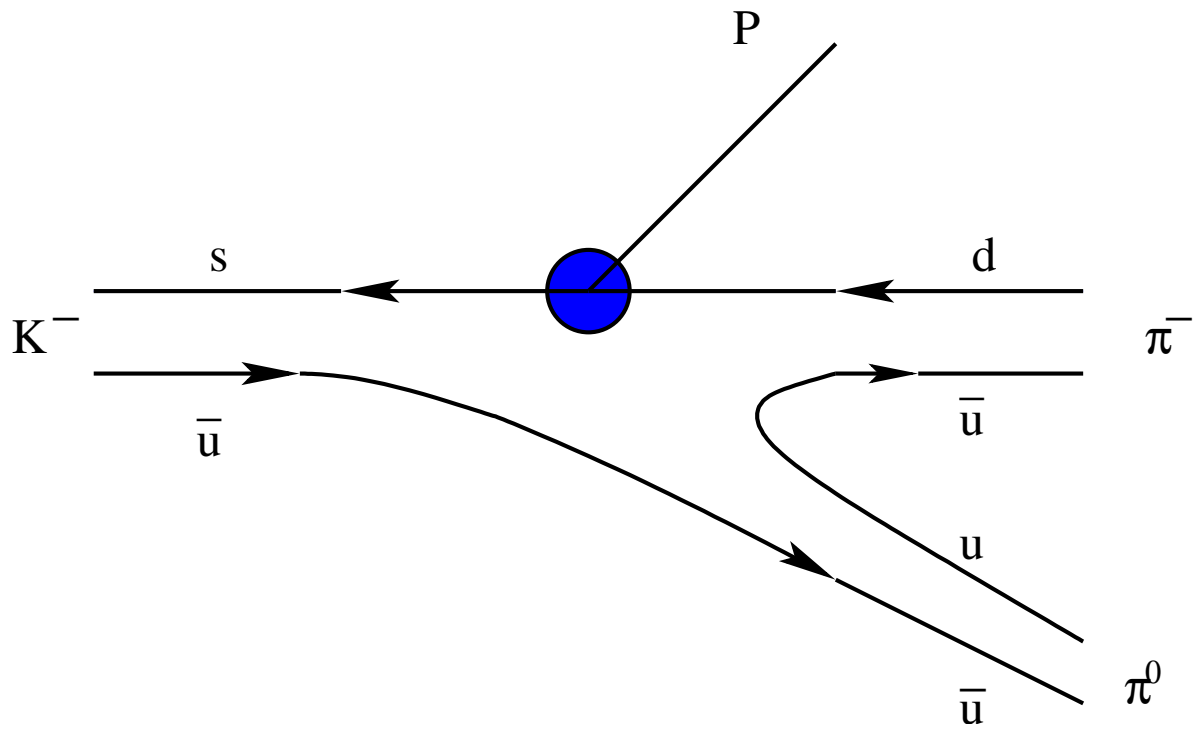
Figure 1: K^- decay into sgoldstino and pions.
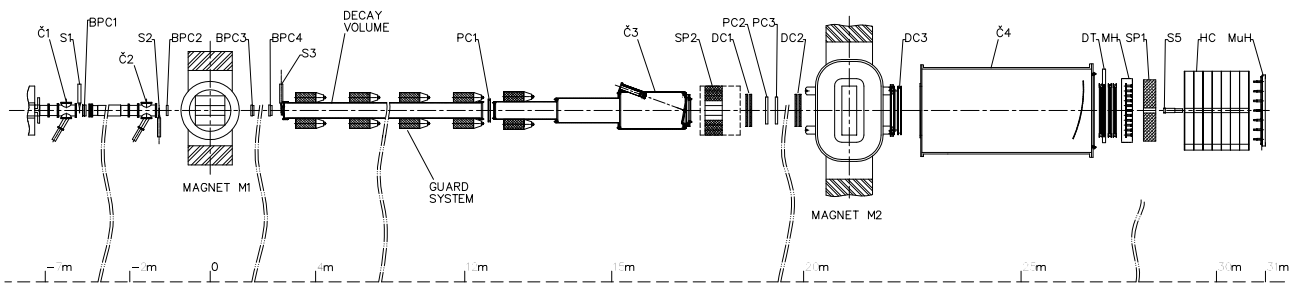
Figure 2: Schematic view of the ISTRA+ setup.
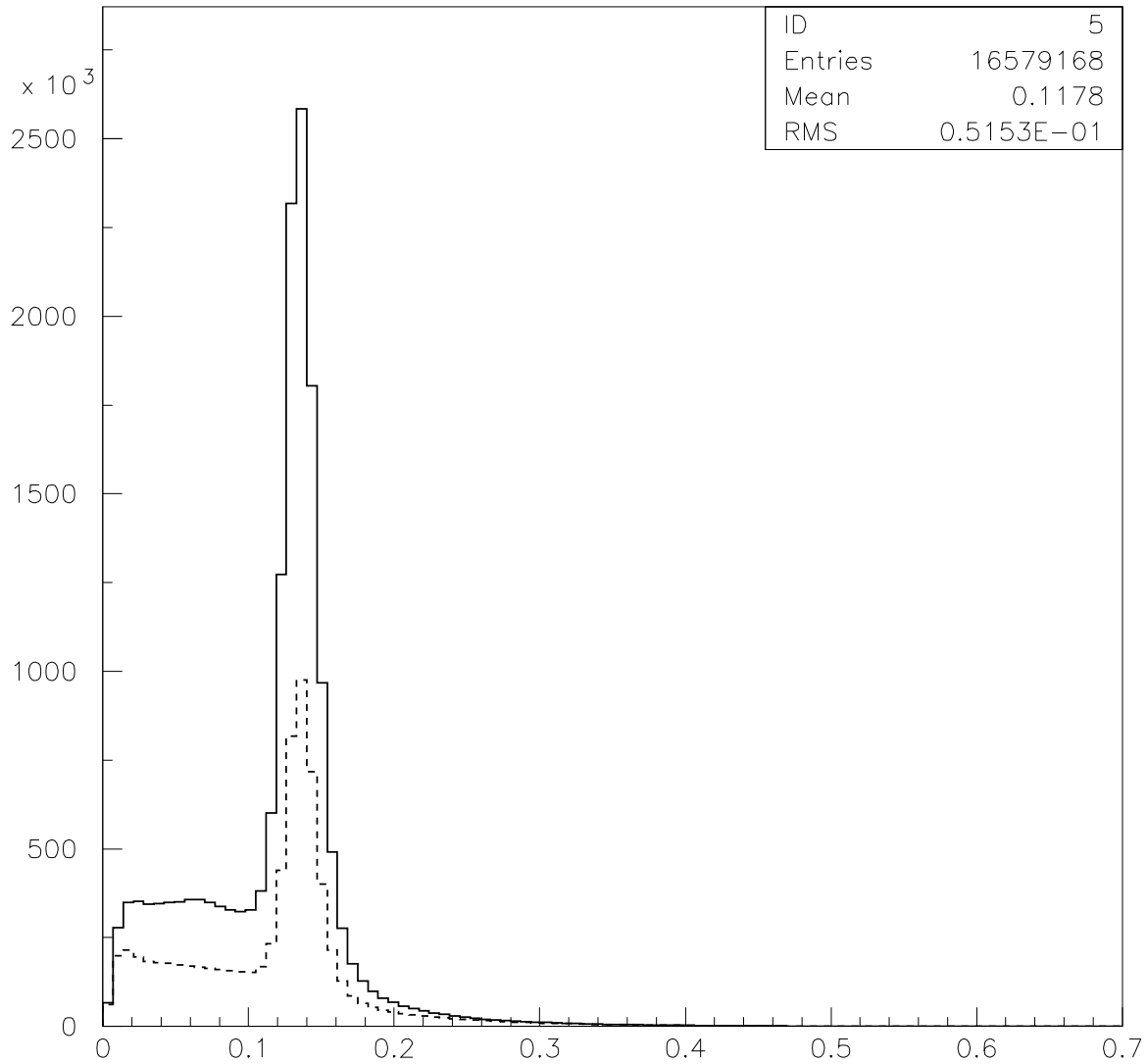
Figure 3: Two photon effective mass spectra for events with one charged track and two showers in the SP_1. Dashed line — first run data, solid line — second run data.
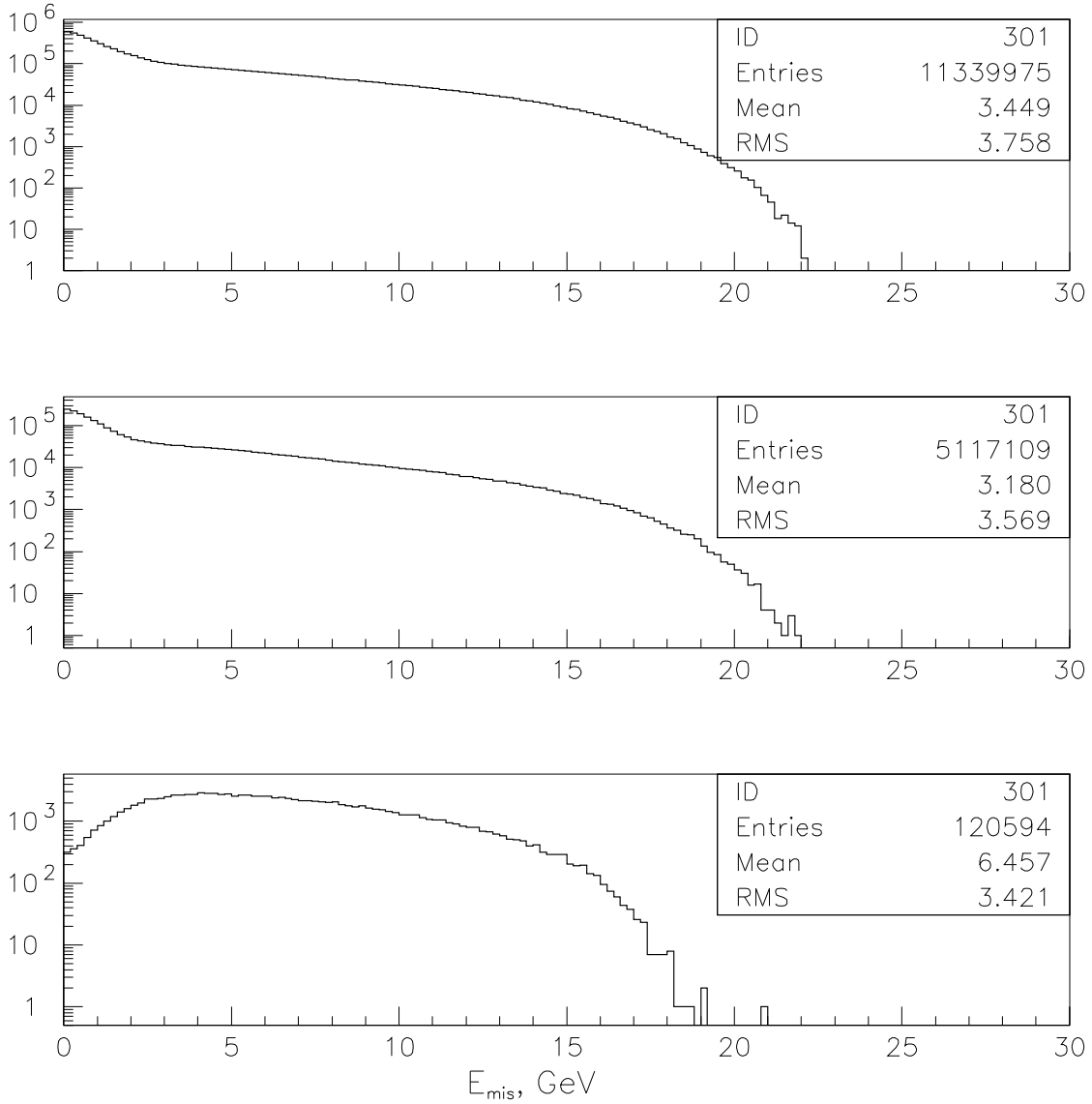
Figure 4: Missing energy spectra, second run data. Upper histogram — real data, middle histogram — background MC events, lower histogram — signal MC events for $m_P = 90$ MeV.
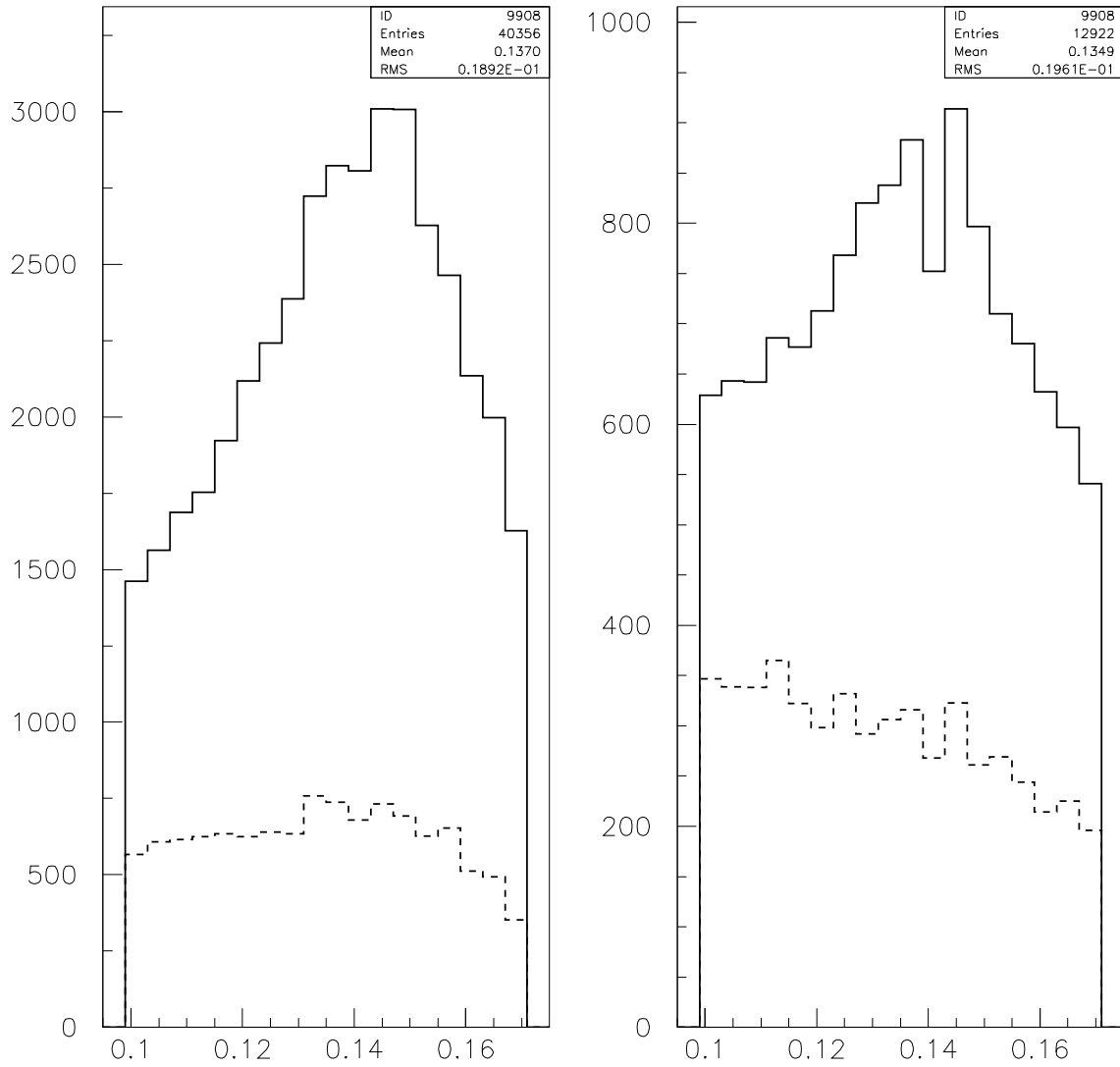
10

Figure 5: The influence of the "Veto" cut on the two-photon effective mass spectrum. Left part — second run, right part — first run; solid line — before the "Veto" cut, dashed line — after the "Veto" cut.
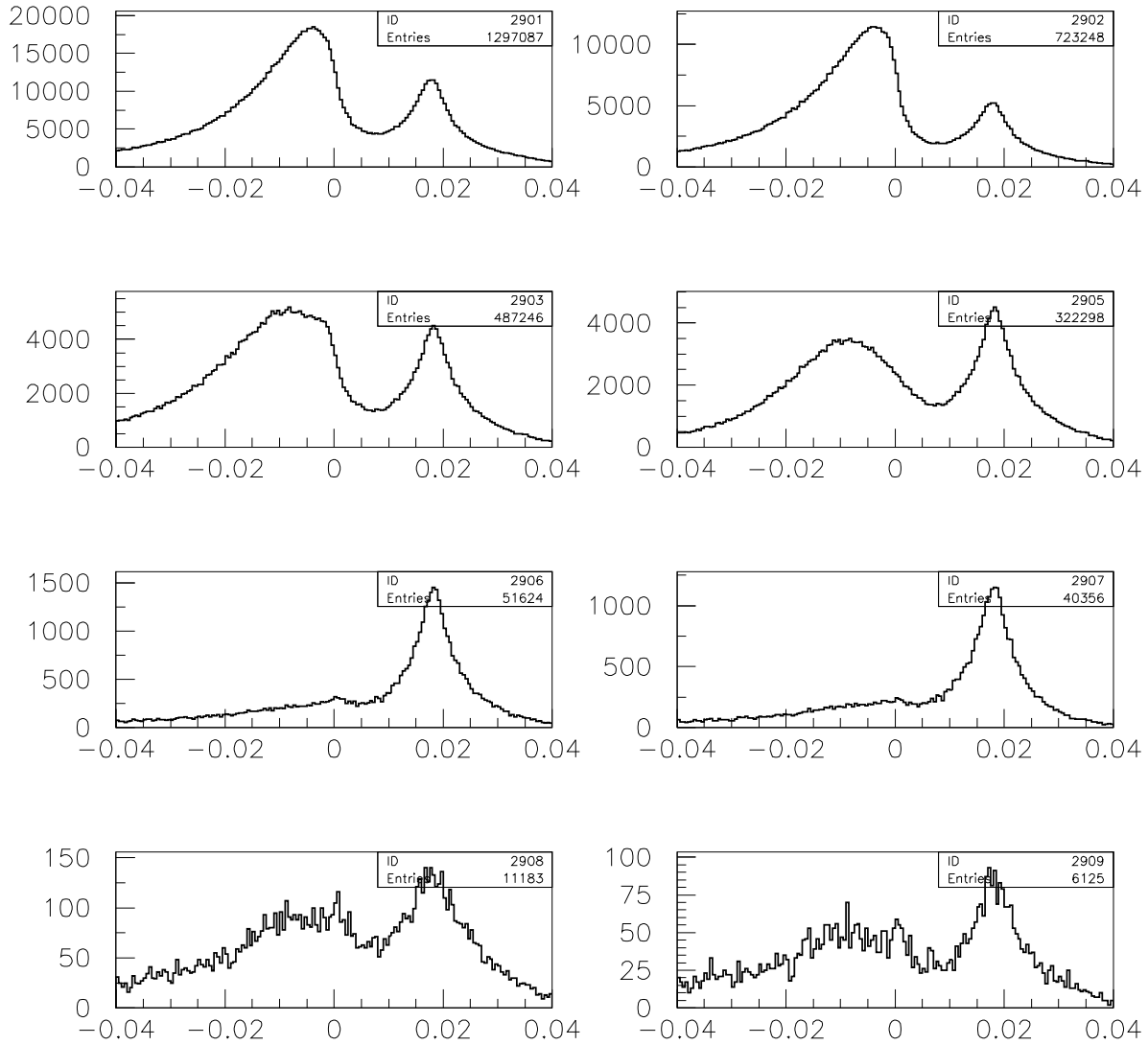
11

Figure 6: Missing mass squared distributions, real data, for successive cuts 3—10 respectively, second run data.
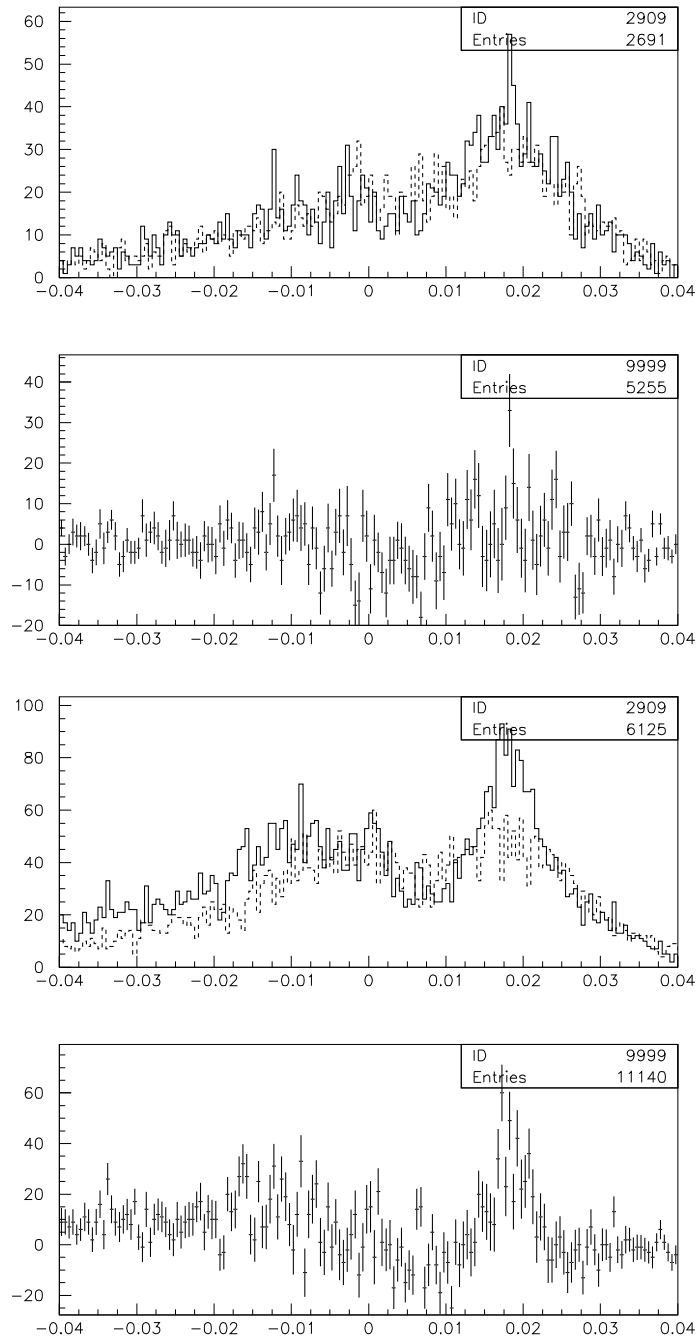
Figure 7: Missing mass squared spectra, background subtraction, first run — upper part, second run — lower part. Solid line shows spectrum for the neutral pion selection within narrow interval, dotted line shows spectrum for tails. Lower histogram in each part shows the difference.
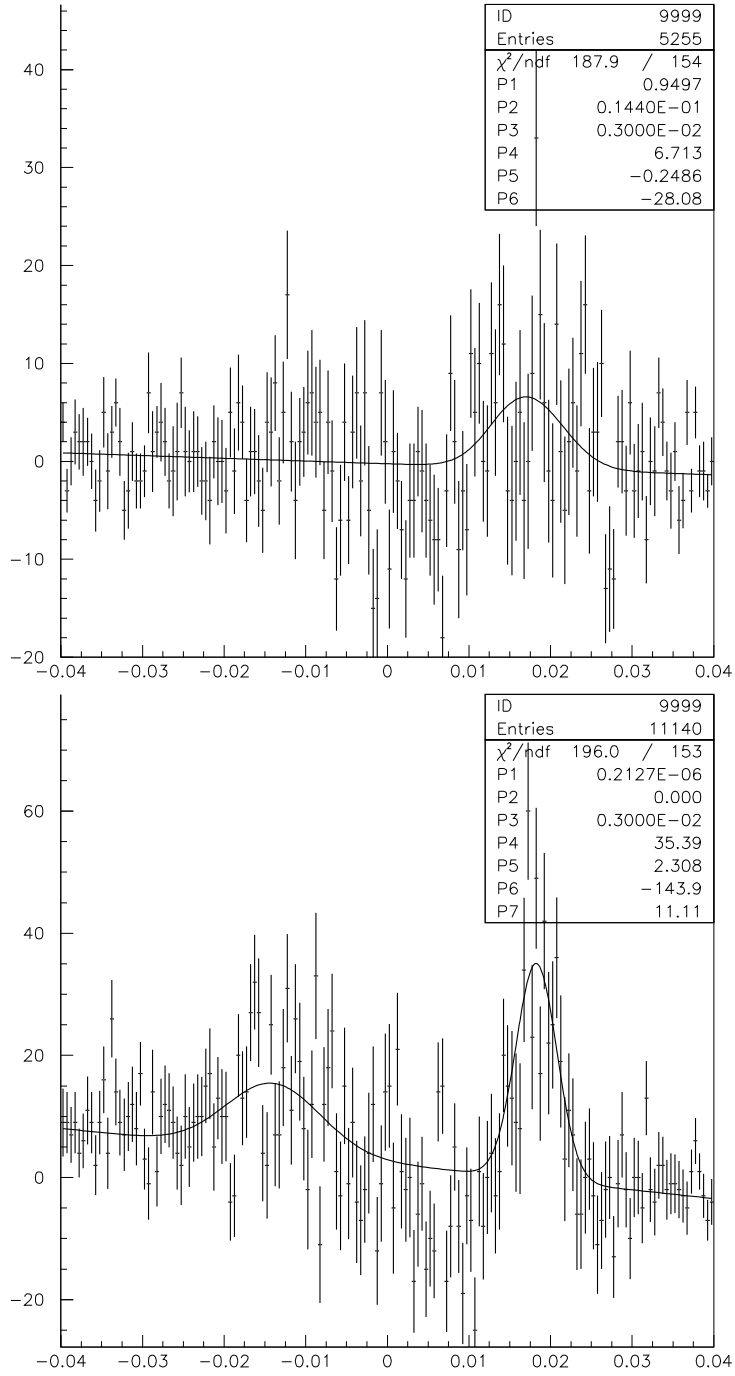
13

ID	9999
Entries	5255
χ^2/ndf	187.9 / 154
P1	0.9497
P2	0.1440E−01
P3	0.3000E−02
P4	6.713
P5	−0.2486
P6	−28.08

ID	9999
Entries	11140
χ^2/ndf	196.0 / 153
P1	0.2127E−06
P2	0.000
P3	0.3000E−02
P4	35.39
P5	2.308
P6	−143.9
P7	11.11

Figure 8: Fit of the missing mass squared spectrum with sgoldstino signal at 120 MeV, first run data, upper part. Lower part — fit of the missing mass squared spectrum with sgoldstino signal at 0 MeV, second run data.
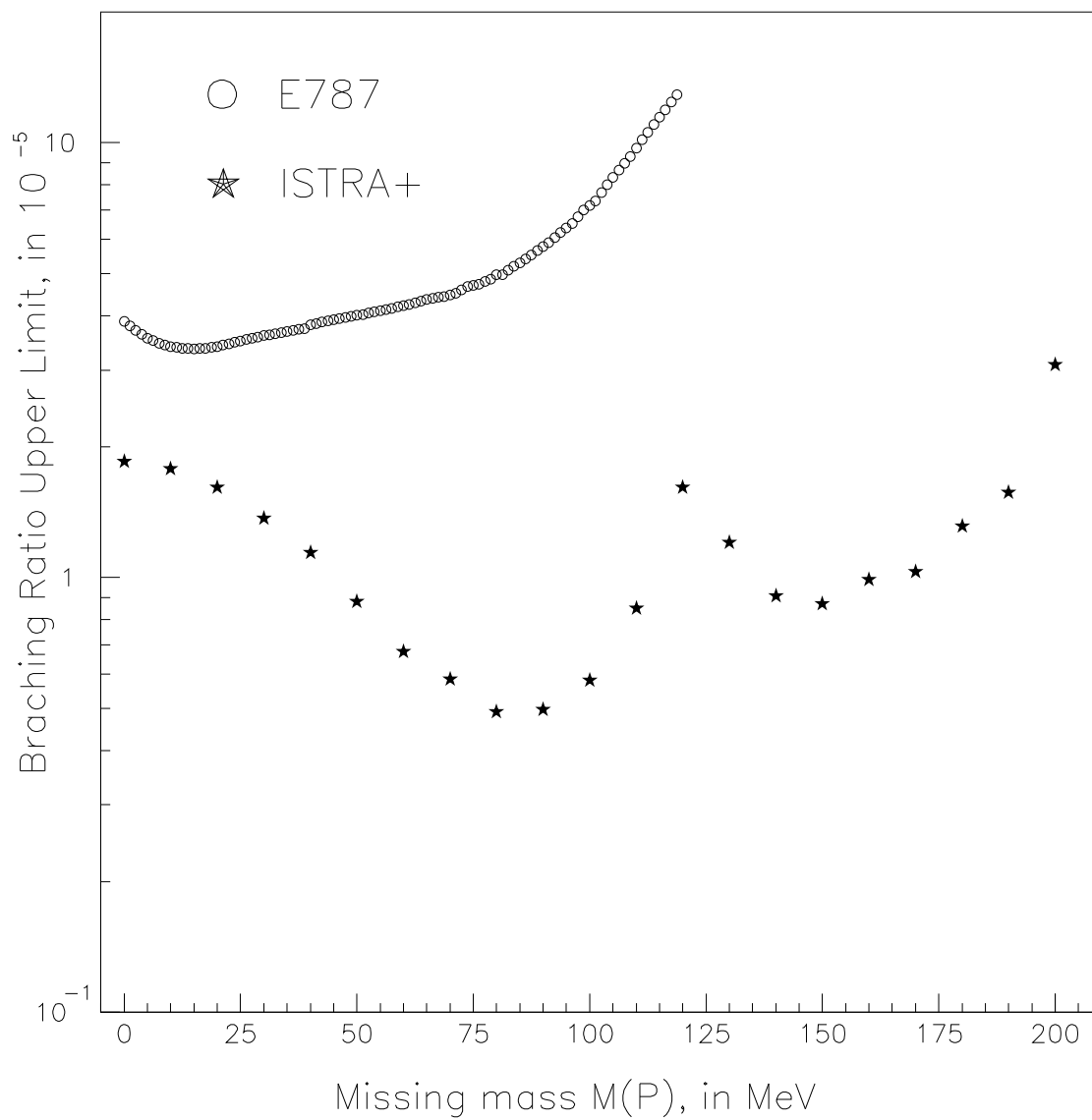
Figure 9: Mass dependence of the upper limits, calculated using two runs together.